Ultrafast amplitude modulation for molecular and hemodynamic ultrasound imaging

Claire Rabut[1], Di Wu[2], Bill Ling[1], Zhiyang Jin[2], Dina Malounda[1], Mikhail G. Shapiro[1,*]

1. Division of Chemistry and Chemical Engineering, California Institute of Technology, Pasadena, CA 91125, USA
2. Division of Engineering and Applied Science, California Institute of Technology, Pasadena, CA 91125, USA

*Corresponding author: mikhail@caltech.edu

SUPPLEMENTARY MATERIAL

MATERIAL AND METHODS

uAM transmission sequence

Three ultrasound bursts of modulated amplitude +1, +½, +½, each carrying N successive tilted plane waves are transmitted into the medium one after the other by a linear ultrasound probe with elements along the x-axis, with a reception time separating each burst (**Fig.1.c.i**). These amplitude-modulated multiplane bursts can be written as:

$$TX(x,t) = TX_a(x,t) + TX_o(x,t+dt) + TX_e(x,t+2xdt) \quad (\textit{Equ. S1})$$

where TX_a, TX_o, TX_e of respective amplitude +1, +½ and +½, each represent the time delay laws of the N successive tilted emissions of different angles $[\alpha_i]_{i=1:N}$ (**S1** for N=8). The half amplitude pulses are achieved by silencing the odd (for TX_o) or even (for TX_e) elements of the ultrasound probe. *dt* is the time delay between bursts. Within each burst, pulses are emitted one after the other with a delay corresponding to 3 wavelengths between each pulse. τ_i is the time delay of the emission of the pulse α_i after the transmission of the first pulse α_1.

AM radio-frequency (RF) data are generated by subtracting the two backscattered signals elicited by the half-amplitude bursts from the signal elicited by the full amplitude burst. To ensure the largest differential response, the full amplitude burst is set to drive GVs into their nonlinear buckling regime[13] while the half-amplitude bursts elicit a linear response (**Fig.1.a-b**). We will see later that with the same received data, we can also obtain linear images by summing the contribution of all the received signals (**Fig.1.c.vi**).

The TX triple-transmission is repeated N times (matching the number of angles), with the only difference between the N TX repetitions being the polarization of successive transmitted amplitudes. To obtain an orthonormal basis of TX matrices, the vector $[\text{TX TX TX } \ldots. \text{ TX}]_N$ is multiplied by the Hadamard Matrix of order N. Hadamard matrices only being of order $N = 2^m$, $[m \in \mathbb{N}]$, the number of angles used in uAM imaging is restricted to values of 2^m. **Fig.1.c-i** illustrates the transmission paradigm of uAM with N = 4 angles. A total of 48 pulses is transmitted in bursts of 4, the burst repeated at 3 different amplitudes and 4 different polarity patterns given by the columns of the Hadamard matrix of order 4.

Hadamard summation and nonlinear artifacts

In MPW processing, the Hadamard-coded received signals are summed following the combination given by the Hadamard matrix lines. Assuming linear scatters only, the summation of the received signals results in N new ultrasound images, corresponding to backscattered echoes of individual plane waves, but with a virtual amplitude N times greater than that received with a single plane wave.

In AM imaging, the subtraction of the two half-amplitude pulses from the full-amplitude pulse allows the elimination of linear signal and the capture of specifically nonlinear responses. In uAM, these nonlinear signals, produced by trios of modulated MPW bursts, contain Hadamard-coded polarities (**Fig.1.c-ii**). In conventional Hadamard summation, the assumption must be made that that oppositely coded signals sum to zero. However, while this is generally true for linear signals, nonlinear scatterers can produce different echo profiles in response to pulses of opposite polarity that do not cancel each other[19,20]. This phenomenon

is the basis for pulse-inversion imaging[22], and a variety of contrast agents, including GVs, produce pulse-inversion nonlinear contrast[13].
To illustrate the issue created by pulse inversion nonlinearity, we consider Hadamard summing for a uAM sequence of $\mathrm{N} = 4$. We define p as the AM-subtracted echo from a positive polarity pulse (blue pulse in **Fig.1.c.ii**), n as the AM-subtracted echo from a negative polarity pulse (green pulse in **Fig.1.c.ii**) and h as the result of summing $p + n$ (black trace in **Fig.1.c.iii**). The four resulting AM RF data can be written as follows (**Fig.1.c.ii**):

$$\begin{aligned} RF_1 &= p(t) + p(t+\tau_2) + p(t+\tau_3) + p(t+\tau_4) \\ RF_2 &= p(t) + n(t+\tau_2) + p(t+\tau_3) + n(t+\tau_4) \\ RF_3 &= p(t) + p(t+\tau_2) + n(t+\tau_3) + n(t+\tau_4) \\ RF_4 &= p(t) + n(t+\tau_2) + n(t+\tau_3) + p(t+\tau_4) \end{aligned} \qquad \textit{(Equ. S2)}$$

The subtraction and addition of this RF data according to the coefficients of the Hadamard matrix of order 4 then leads to four new sets of Hadamard RF data $H_1, \ldots, H_4$:

$$\begin{aligned} H_1 &= RF_1 + RF_2 + RF_3 + RF_4 \\ H_2 &= RF_1 - RF_2 + RF_3 - RF_4 \\ H_3 &= RF_1 + RF_2 - RF_3 - RF_4 \\ H_4 &= RF_1 - RF_2 - RF_3 + RF_4 \end{aligned} \qquad \textit{(Equ. S3)}$$

This results in the transformed RF data (**Fig.1.c.iv**):

$$\begin{aligned} H_1 &= 4 \cdot p(t) + h(t+\tau_2) + h(t+\tau_3) + h(t+\tau_4) \\ H_2 &= 4 \cdot p(t+\tau_2) \\ H_3 &= 4 \cdot p(t+\tau_3) \\ H_4 &= 4 \cdot p(t+\tau_4) \end{aligned} \qquad \textit{(Equ. S4)}$$

It can be seen from this result that Hadamard subtractions/additions result in the desired positive single-wave signals of quadruple amplitude for $H_2 \ldots . H_4$, but that H_1 contains both a quadruple-amplitude signal at t and nonlinear signals h at $(t+\tau_2)$, $(t+\tau_3)$, $(t+\tau_4)$ due to the pulse inversion operation. This artifactual signal results in the spatial mis-assignment of nonlinear signal during subsequent coherent compounding. This pattern generalizes to higher-order Hadamard matrices. Undesirable nonlinear pulse inversion signals always appear in H_1, and never in $H_{>1}$. For any MPW sequence of N angles, we have after Hadamard summing of the nonlinear raw data:

$$\begin{aligned} H_1 &= N \cdot p(t) + \ldots + h(t+\tau_N) \\ H_2 &= N \cdot p(t+\tau_2) \\ &\ldots \\ H_N &= N \cdot p(t+\tau_N) \end{aligned} \qquad \textit{(Equ. S5)}$$

Selective coherent compounding
Based on *Equ. 4* derived above, a *selective coherent compounding* of all Hadamard RF data except the first one (H_1) is then performed giving the compounded data set C:

$$C = \sum_{i=2}^{N} H_i(t - \tau_i) \qquad \textit{(Equ. S6)}$$

C is then beamformed (delay-and-sum algorithm) and a final nonlinear image $S(K_x, K_z)$, (K_x and K_z being the respective lateral and axial dimensions of the final image) is finally obtained.

Near field in uAM imaging

In ultrasound imaging, the simultaneous excitation of all the elements of a transducer is assumed to create an acoustic plane wave by interference of the simultaneously-emitted pulses in front of the probe. In order to create two acoustic plane waves of full and half amplitude for uAM imaging, we proposed to emit simultaneously (or with a time delay with respect to each other, to « tilt » the plane waves) ultrasound pulses with all of the 128 elements of the probe (spaced by 0.1 mm), or with every other element (half of them: 64 elements, spaced by 0.2 mm). In the uAM pulse sequence, two half-amplitude fields are created, with the odd and the even elements of the probe. These two half-amplitude fields are then summed to virtually create a full-amplitude acoustic field that is finally subtracted from the field obtained with 128-elements.

We simulated the plane wave formation in front of the probe under the different transmission conditions of uAM (all or half of the elements emitting) using k-wave (open-source acoustics toolbox for MATLAB). We simulated wave propagation in a homogeneous and isotropic medium (water): the speed of sound was set to 1480 m/s. The size of the domain was 12.8 mm × 12.8 mm and was discretized with a step size of 50 µm; perfectly matched layers were used to absorb the waves at the edges of the domain; 128 transducer elements were positioned 1 mm from the top of the domain and positioned horizontally 0.1 mm from each other. The source broadcasted a short pulse (1 cycle) with a central frequency of 15 MHz. **Fig.S4.a** shows the propagation of the acoustic field after simultaneous emission by all of the 128 elements (Pressure field: P_a), while **Fig.S4.b** shows the propagation of the acoustic field after simultaneous emission by 64 elements only (the odd elements, pressure field: P_o), spaced by 0.2 mm. In a third simulation (not shown), we calculated the resulting acoustic field obtained after emission by the 64 even elements of the transducer (pressure field: P_e). We then compared the resulting maximum pressure fields at different depths obtained with P_a or with the sum of P_o+ P_e (**Fig.S4.c**). The resulting wave in front of the probe is mostly planar between the lateral coordinates [+1mm ; +11.8mm], outside of the edge effect regions on the array's extremes. In this analysis, the mean value of the maximal received pressure at a given depth and the standard deviation of the horizontal pressure fields is calculated between these coordinates.

In the near field (which will be defined by the end of this section), the sum of the two half-amplitude fields don't equal the full-amplitude field. At 1 mm depth, for example (**Fig.S4.c)**, the maximum pressure field is substantially higher for P_o+ P_e than for P_a. This observation is confirmed **Fig.S4.d**, which shows that the mean P_o+ P_e maximal pressure at depth 1 mm is 723 kPa whereas the maximal P_a pressure is averaged around 618 kPa. However, at greater depth, the averaged field P_o+ P_e gets closer to the mean value of the field P_a. At a depth of 2.7 mm, P_o+ P_e = 638 kPa and P_a = 636 kPa, the difference being below 0.4%. With less than 0.5% difference, we consider the two fields as substantially equal.

We also considered the standard deviation of the pressure field (along the horizontal axis) as a function of the depth. At each depth, we evaluated the ratio of the standard deviation and the mean pressure value $P_o + P_e$ and P_a (**Fig.S4.e**). Close to the probe (< 2.5 mm depth), the standard deviation ratio of the pressure field is higher for $P_o + P_e$ (>4%) than for P_a (<2%). At 2.6 mm, this ratio for $P_o + P_e$ drops to 1.7% and equates to the ratio of P_a within an accuracy of 0.03%.

We define the near field in uAM imaging as the depth for which the pressure fields created by all (128), or by the sum of the odd (64) and the even (64) elements generate equal maximum peak values (averaged along the horizontal line defined by the depth) within an accuracy of 0.5% and for which the standard deviations (for each transmission condition) of the maximum pressure field at this depth represent less than 2% of the average pressure. At 15 MHz, with a 0.1 mm pitch ultrasound probe, the near field in uAM is therefore 2.6 mm.

Spatial resolution calculation

The ultrasound phantom for quantifying the resolution of the imaging techniques was prepared by embedding GVs in 1% (w/v) agarose gel in PBS. GVs were incubated at 42°C and mixed in a 1:1 ratio with molten agarose for a final GV concentration of 1 OD500nm and loaded into a custom rectangular mold. To make the pattern of repeated lines of intact GVs (**Fig.S3.a**), a 3.7MHz acoustic standing wave was applied to the phantom using a custom device such that the peak positive pressure at the pressure antinodes of the standing wave exceeded the critical collapse pressure of the GVs[31]. The driving pressure was selected such that the line pattern generated by the remaining intact GVs was less than 100 µm in width. The ground truth of the patterned GVs was imaged using brightfield optical imaging (**Fig.S3.b**), and quantified using ImageJ, the full width at half-maximum (averaged across N=13 lines) was measured as 60 µm. We positioned the phantom in a water bath with the lines being oriented horizontally, and imaged it successively with pAM, xAM and uAM (**Fig.S3.c**). We repeated the imaging protocol by flipping the phantom of 90º and imaged the vertical lines (**Fig.S3.d**). The spatial axial and lateral resolutions of each pulse sequence were calculated by evaluating the full width at half-maximum of the horizontal (axial resolution) and vertical (lateral resolution) lines (averaged over 20 lines and 10 time points).

Linear processing

All the received RF data are stored in the ultrasound scanner, allowing multiple different signal processing operations in addition to nonlinear imaging. For linear imaging, we sum the full and half-amplitude pulses instead of subtracting them (**Fig.1.c.vi**) and repeat the remaining post-acquisition processing described in the previous section. This results in B-mode ultrasound images, free from nonlinear artifacts thanks to selective coherent compounding.

Dynamic processing of ultrafast images

Ultrasound plane wave imaging enables ultrafast scanning of the media[16]. The ultrafast repetition of the uAM pulse sequence therefore provides access to fast transient linear and nonlinear events in the whole imaging plane. In two example applications of this capability, we applied a clutter filter to the spatiotemporal data[23] to detect fast flows in the imaging planes.

Ultrasound acquisition sequence

Ultrasound sequences were implemented on a research ultrasound scanner (Verasonics, USA) using an ultrasound probe with 128 linear elements emitting at 15.625 MHz (pitch = 0.10 mm). The acquisition scripts and processing codes were written in Matlab (Matworks, USA).
We used a Verasonics Vantage ultrasound system with an L22-14v probe (Verasonics Inc., Redmond, WA, USA) to implement the uAM, xAM and pAM imaging sequences. The probe is a linear array of 128 elements with a 0.10-mm pitch, an 8-mm elevation focus, a 1.5-mm elevation aperture, and a center frequency of 18.5 MHz with 67% −6 dB bandwidth. We applied a single-cycle transmit waveform at 15.625 MHz to each active array element to ensure our fundamental frequency is divided 4 times with the 62.5-MHz sampling rate of the system. For the uAM sequence, we use the full aperture of the probe, i.e., 128 elements, to send the successive plane waves. For xAM, to reproduce the optimal results published in Maresca et al.[15], we used an aperture of 65 elements for the xAM sequence. For pAM, we used an aperture of 89 elements. The input voltage driving the transducer was set in order to reach, for each modality, a peak positive pressure of 500kPa.

Framerate evaluation for pAM, xAM and uAM

For a 10mm depth acquisition, theoretically acquired along the 128 elements of a transducer linear array:
One xAM image is acquired after the transmission along each vertical line of an image of three distinct pulses. In xAM these three pulses correspond to the two individual and one cross propagating plane wave.
One image is then acquired in:

$t = \sqrt{(number\ of\ vertical\ lines * pitch)^2 + depth^2} / speed\ of\ sound$ (*Equ. S7*)

with: $number\ of\ vertical\ lines = 128$, $pitch = 0.10\ mm$, $depth = 10\ mm$ and $speed\ of\ sound = 1540\ m/s$

so: $t = \sqrt{(128 * 0.100)mm^2 + 10mm^2} / 1540\ ms^{-1} = 10.5\ \mu s$

Then, one image of 128 vertical lines can theoretically be acquired in: $T_{image}(xAM) = 10.5\ \mu s \times 3 \times 128 = 4.03\ ms$ which corresponds to an imaging framerate of 250Hz.
The same calculation can be applied for pAM imaging and would result in the same imaging framerate.

One similar uAM image of 128 vertical lines is acquired after the transmission of 3 amplitude modulated sets of 8 multiplane wave bursts. After the emission of the first tilted angle, 2.4 additional microseconds are necessary to transmit the rest of the 8-multiplane wave burst (see **Fig.S1**). A uAM transmission is therefore 2.4 µs longer than a single plane wave transmission. Therefore, the backscattered echoes from the last plane wave of the burst arrive with a delay of 2.4 µs after the echoes coming from the first plane wave of the burst. Then, the uAM transmission/reception period is: 10.5 + 2.4 = 12.9 µs. One uAM-8 image therefore can be acquired in: $T_{uAM} = 12.9\ \mu s \times 3 \times 8 = 0.309\ ms$ which corresponds to an imaging framerate of 3.2kHz.

For the same field of view (width given by the probe: 128 vertical lines of 0.1mm, depth: 10mm), uAM is therefore 3.2/0.250 = 12.8 times faster than conventional xAM or pAM imaging.

These calculations are performed to compare imaging framerates of same-width images acquired by the different techniques. In reality, the imaging aperture used in in our experiments spanned 89 elements of the probe for pAM[15] and 64 elements for in xAM[15]. The imaging

framerate for these narrower images would therefore be proportionally accelerated, but at the cost of smaller field of view. Therefore in practice, as implemented in this study, the number of transmits in uAM is reduced by more than 8-fold compared to pAM or xAM for the formation of one AM image

Preparation of gas vesicles

Nonlinear GVs were prepared as described in Lakshmanan et al.[32]. Briefly, GVs were harvested from buoyant *Anabaena flos-aquae* cells by hypertonic lysis and purified by repeated centrifugally assisted flotation and resuspension. The GVs were stripped of their outer GvpC layer by treatment with 6M urea, followed by additional repeated centrifugally assisted flotation, dialysis in 1x PBS and resuspension to remove the GvpC and urea.

Tissue-mimicking phantoms

Tissue-mimicking phantoms for imaging were prepared by casting 1% (w/v) agarose in PBS with 0.2% (w/v) AlO_3. For static imaging, we used a custom 3D-printed mold to create two rows of cylindrical wells with 2 mm diameter. GVs were incubated at 42 °C for 1 minute and then mixed in a 1:1 ratio with low-melt molten agarose (at 42 °C) for a final GV concentration corresponding to 3 OD500nm and loaded into the phantom. The AlO_3 concentration was chosen to match the scattering echogenicity of the GV well. According to [32], the molarity of GVs is 114 pM/OD. The upper row was centered at 6 mm depth and the lower row at 9 mm.
For dynamic imaging, using a custom 3D-printed mold through which 1 mm diameter tubes are arranged, we mixed in a 1:1 ratio of GVs (OD 2) and molten agarose for a final GV concentration corresponding to 1 OD500 nm and loaded into the phantom. After 20 min, we made sure that the agarose was fully solidified and gently pulled out the tubes leaving 1 mm diameter tunnels crossing the whole agarose phantom. Solutions of PBS or of GVs in suspension (OD 1) were then injected through the tube using a syringe pump at 1 mL/min.

Extracting signal from flowing GVs only during the dynamic in vitro study

To distinguish the flow of GVs from the stationary ones in the agarose phantom in 4ms only with uAM imaging, we performed a SVD decomposition on the 13 uAM-nonlinear images in order to decompose the acquisition into a weighted, ordered sum of separable spatio-temporal modes expressed by **U**, **Δ** and **V** as:

$$\mathrm{uAM(t)} = \sum_i \sigma_i . U_i \otimes V_i \qquad (\textit{Equ. S8})$$

with U_i and V_i the i-th columns of the corresponding SVD matrices **U** and **V**. And **Δ** the weighting matrix. **U** represent the spatial-only modes of the uAM acquisition and **V** the temporal-only modes. Finally, the diagonal matrix **Δ** ranks these modes. As described in [23], removing the first mode(s) from the SVD decomposition allows the extraction of the flow-only from the acquisition. Here, we remove the first mode only and apply an inverse SVD decomposition to reconstruct a 3D (2D space + 1D temporal) acquisition without the background signal component. The PD value PD for each pixel is then calculated as:

$$PD = \frac{1}{N} . \sum_{i=1}^{N} s_{filtered}^2(t_i) \qquad (\textit{Equ. S9})$$

Where N=number of temporal samples in one uAM-doppler block (here N=13) and $s_{filtered}$ is the filtered signal.

In vivo imaging

All animal experiments were conducted under protocols approved by the Institutional Animal Care and Use Committee of the California Institute of Technology. The *in vivo* experiment presented has been performed on a BALB/c female mouse (Jackson Laboratory) aged 7 weeks under a protocol approved by the Institutional Animal Care and Use Committee of the California Institute of Technology. No randomization or blinding are necessary in this study. The mouse was anesthetized with 2%–3% isoflurane, depilated over the imaged region, and imaged using an L22-14v transducer with the uAM pulse sequence. Eight hundred seconds after the start of imaging, 120 µL of OD_{500} 25 GVs were infused over 10s. The acquisition continued for 2000 s after injection.

In vivo PD processing from uAM-doppler acquisitions

Power Doppler visualizes the concentration of moving blood cells during a determined time interval ΔT. This integration time should cover several cardiac cycles in order to average the heartbeat dynamic. The averaged heartbeat frequency in mice is estimated at 10 Hz. A time interval ΔT = 400 ms is therefore adequate to average approximately four heartbeats. uAM images were acquired at 500 Hz, which is equivalent to 200 images during 400 ms, with one uAM-doppler block repeated every 8 s. To extract the signal from the blood stream only (in which both red blood cells and GVs contribute to the signal), linear processing is performed on the received AM data after transmission of the uAM pulse sequence: instead of subtracting the half-amplitude pulses from the full-amplitude pulses for nonlinear processing, the summation of the AM backscattered echoes is performed to conserve the linear components of the ultrasound image (**Fig.1.c.vi**). A clutter filter as described in the dynamic *in vitro* study and in [24] is then applied to each of the uAM linearly-processed blocks (of 200 images acquired at 500Hz) to extract the blood signal from the spatiotemporal acquisition. For this study, the first 50 SVD modes were removed from the SVD decomposition. The PD value PD for each pixel is then calculated as:

$$PD = \frac{1}{N}.\sum_{i=1}^{N} s_{blood}^2(t_i) \qquad (\textit{Equ. S10})$$

Where N=number of temporal samples in one uAM-linear doppler block (here N=200) and s_{blood} is the filtered blood signal.

A similar processing scheme could be applied to nonlinear uAM-nonlinear doppler images (images obtained after subtraction of the half-amplitude pulses from the full amplitude ones to conserve the nonlinear components of the image only) and will therefore express the PD of moving GVs only (**S2**):

$$PD_{GVs} = \frac{1}{N}.\sum_{i=1}^{N} s_{nonlinear}^2(t_i) \qquad (\textit{Equ. S11})$$

SUPPLEMENTARY FIGURES

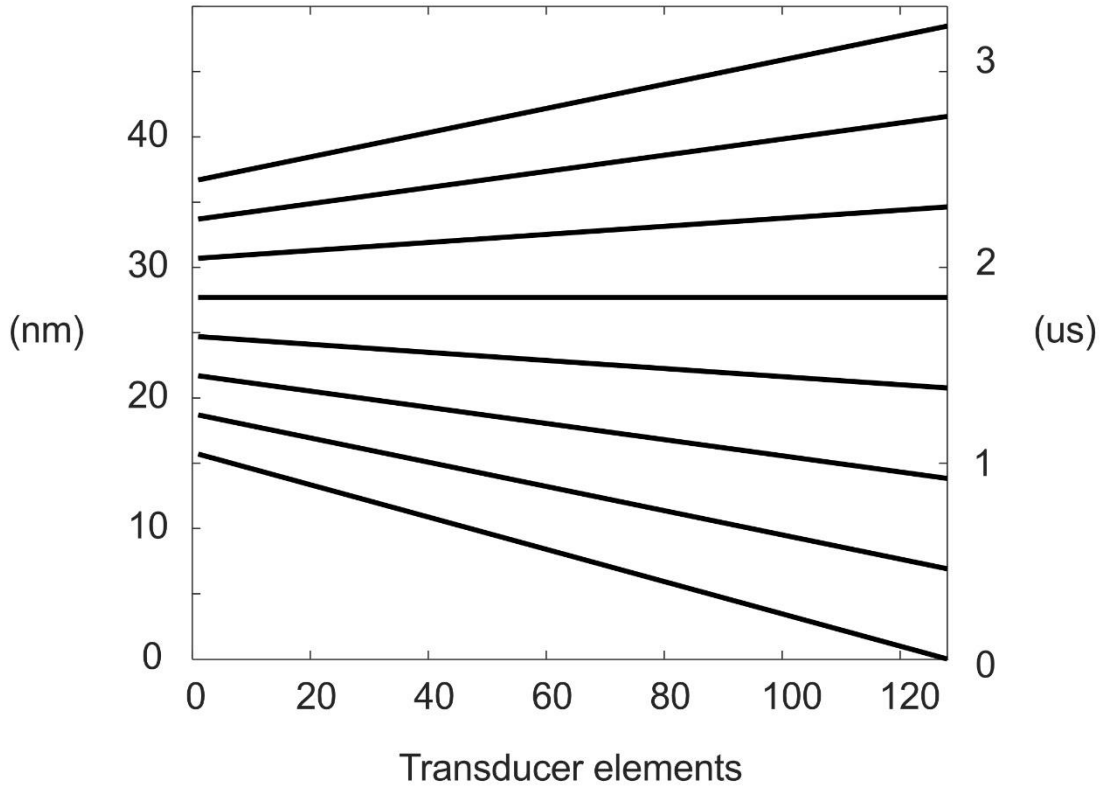

FIG.S1: Time delay law of one 8-angle burst of the uAM transmission sequence.

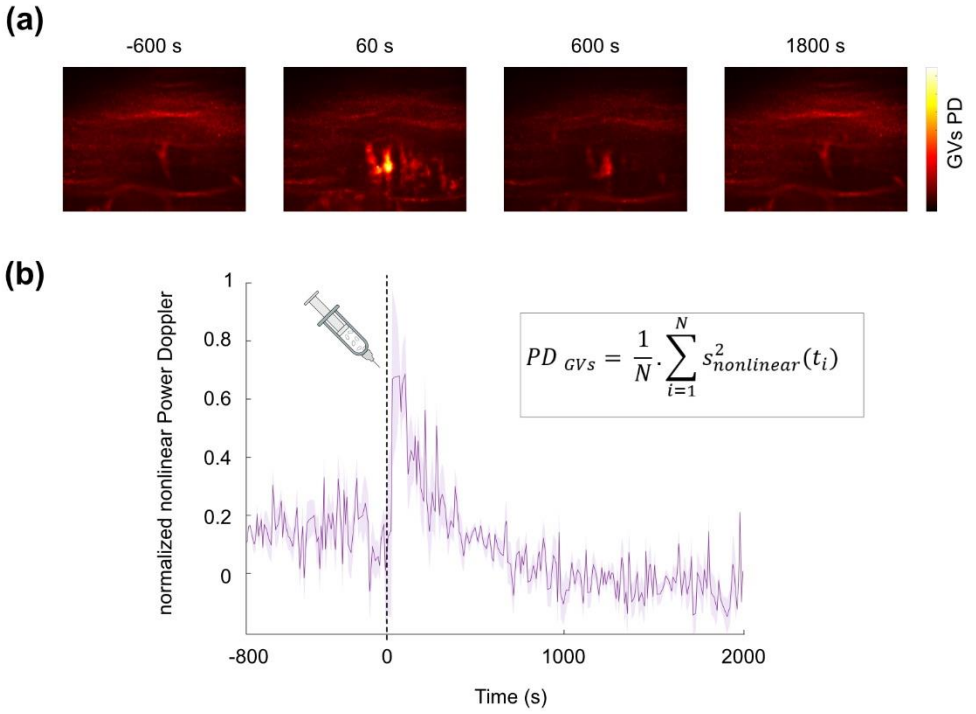

FIG.S2: Power doppler processing of the nonlinear signal during mouse liver imaging*. (a) The power Doppler images illustrates the absence of circulating GVs before injection (-600s), the uptake of GVs right after injection (60s) and clearing of GVs from the blood stream despite the presence of GVs in the liver (>600s). (b) Nonlinear PD time course within the liver.*

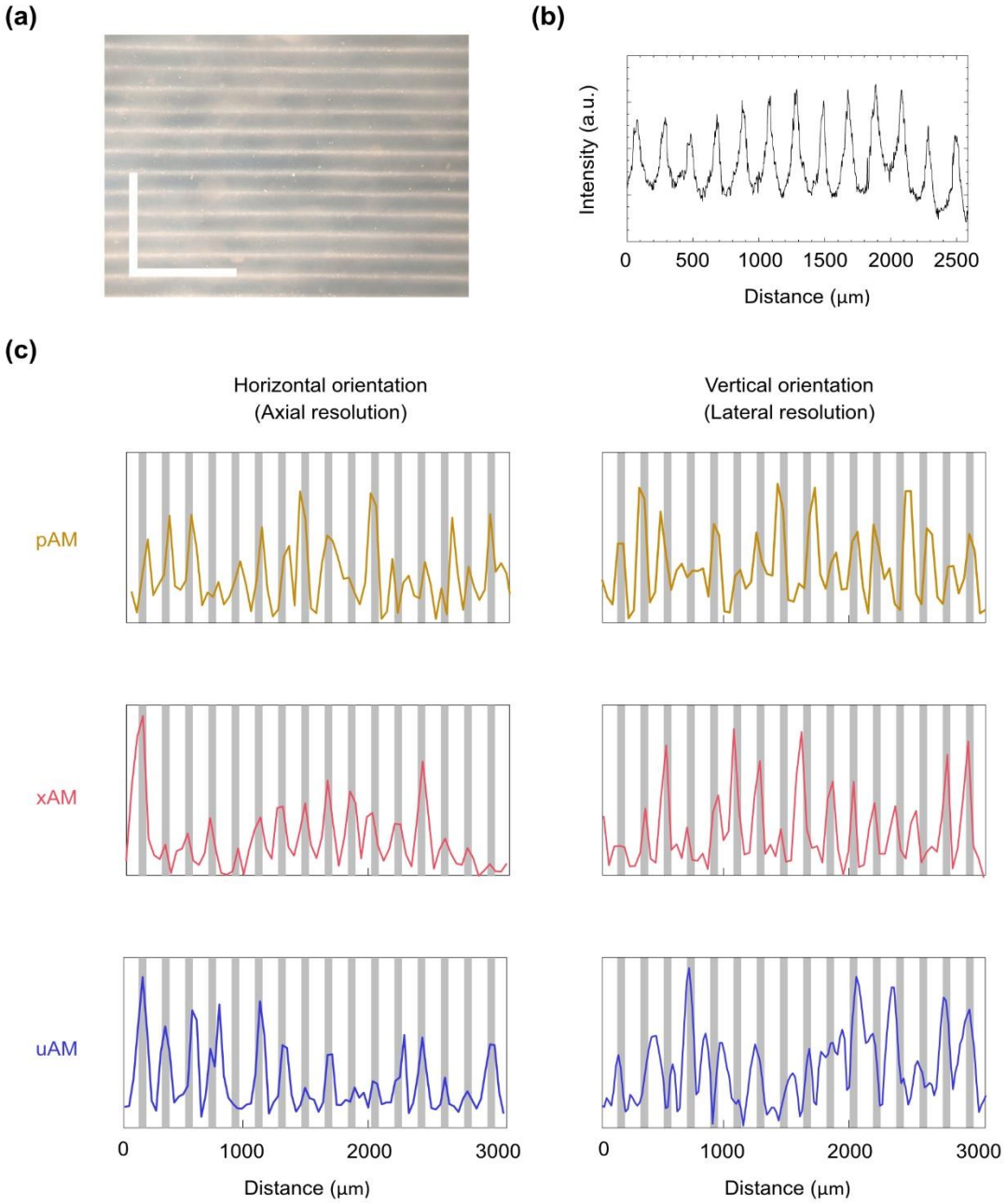

FIG.S3: Spatial resolution estimation of pAM, xAM and uAM imaging using an agar phantom with repeated lines of intact GVs. *(a) Bright field optical imaging of the agar phantom. White lines correspond to GVs. Scale bar: 1 μm (b) Optical intensity profile measured along a single line of the phantom. The ground truth of the patterned GVs was quantified using ImageJ: the full width at half-maximum was measured as 60 μm (c) pAM, xAM and uAM intensity profile of the phantom in the horizontal, and vertical orientation.*

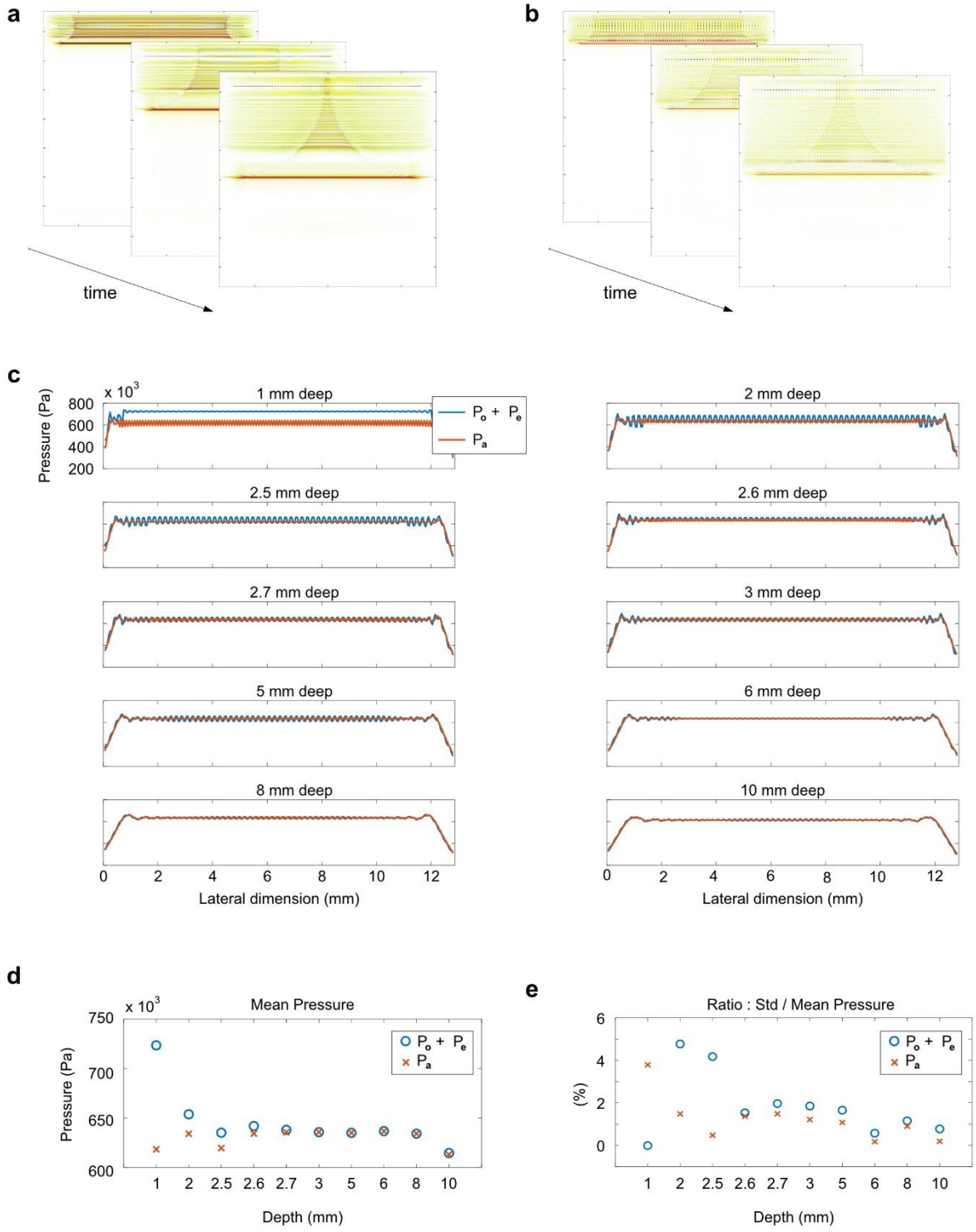

FIG.S4: Acoustic pressure field K-wave simulation of plane waves generated with 128 or 64 elements. *(a) k-wave spatio-temporal simulation of the acoustic field P_a created by the simultaneous emission of the 128 transducer elements of an ultrasound probe (15MHz pulse, 1 cycle, pitch 0.1 mm). (b) Spatio-temporal simulation of the acoustic field created by the simultaneous emission of 64 elements of the same ultrasound probe (P_o : odd elements only, now spaced by 0.2 mm). (c) Lateral pressure profiles of the maximum received pressures at different depths: P_a corresponds to the pressure propagating after emission by the 128*

elements of the probe. P_o+ P_e corresponds to the sum of the pressures from the odd (64 elements) and even (64 elements) elements of the probe. (d) Mean lateral pressure at different depths calculated between the lateral coordinates +1 mm and +11.8 mm of the probe e. Ratio of the standard deviation (Std) and the mean lateral pressure calculated between +1 mm and +11.8 mm.

ADDITIONNAL REFERENCES

[30] D. Wu., D. Baresch, C. Cook,D. Malounda, D. Maresca, M.P. Abundo, D.R. Mittelstein, M. G. Shapiro, " Genetically Encoded Nanostructures Enable Acoustic Manipulation of Engineered Cells". bioRxiv 691105 (2019)

[31] A. Lakshmanan, G. J. Lu, A. Farhadi, S.P. Nety, M. Kunth, A. Lee-Gosselin, D. Maresca, R.W. Bourdeau, M. Yin, J. Yan, C. Witte, D. Malounda, F.S. Foster, L. Schröder, M.G. Shapiro, " Preparation of Biogenic Gas Vesicle Nanostructures for Use as Contrast Agents for Ultrasound and MRI". Nat Protoc 12 (10), 2050–2080 (2017)